J Intell Robot Syst (2009) 56:389–423
DOI 10.1007/s10846-009-9324-z

Realization of Dynamic Stair Climbing for Biped Humanoid Robot Using Force/Torque Sensors

Jung-Yup Kim · Ill-Woo Park · Jun-Ho Oh

Received: 25 December 2007 / Accepted: 30 March 2009 / Published online: 29 April 2009

Abstract This paper proposes a control algorithm for the dynamic stair climbing of a human-sized biped humanoid robot. Dynamic stair climbing can cause more instability than dynamic biped walking on the ground because stair climbing requires an additional vertical motions and a large step length. We assume that stair configuration is already known and only use force/torque sensors at ankle joint to achieve a control algorithm for a stable dynamic stair climbing. We describe a stair climbing pattern generation and stair climbing stages, and then propose a real-time balance control algorithm which is composed of several online controllers. Each online controller is addressed in detail with experimental results. Finally, the effectiveness and performance of the proposed control algorithm are verified through a dynamic stair climbing experiment of KHR-2.

Keywords Dynamic stair climbing · Real-time balance control · Biped humanoid robot · KHR-2 · Force/torque sensor

J.-Y. Kim
Humanoid Robot Research Laboratory, School of Mechanical Design and Automation Engineering, Seoul National University of Technology, 138 Gongrung-gil, Nowon-gu, Seoul 139-743, South Korea
e-mail: jyk76@snut.ac.kr

I.-W. Park (✉)
Department of Information and Control Engineering, Kwangwoon University, 447-1, Wolgye-dong, Nowon-gu, Seoul 139-70, South Korea
e-mail: mrquick@kw.ac.kr

J.-H. Oh
HUBO Laboratory, Humanoid Robot Research Center, Department of Mechanical Engineering, Korea Advanced Institute of Science and Technology, 373-1 Guseong-dong Yuseong-gu, Daejeon 305-701, South Korea
e-mail: jhoh@kaist.ac.kr

1 Introduction

Dynamic biped walking is the most fundamental ability of biped robots. In general, most researchers of biped robotics society have focused on the realization of stable biped walking, and have established their own control strategies. At present, many biped humanoid robots have succeeded in stable dynamic walking [1–5]. Generally, the control strategies of dynamic walking of biped robots have been based on walking pattern generation and online balance control. Walking pattern has been usually designed by solving Zero Moment Point (ZMP) dynamics in order to generate a desired ZMP trajectory. Online balance control is necessary to compensate ZMP error which is caused by the unevenness of the ground surface, sensing noise, and imperfect dynamic models of the robot. Interestingly, mobile robots that have wheels or caterpillars also can move on ordinary ground with better efficiency, stability, and speed. Of course, biped walking is very attractive considering it adds an element of human-friendliness to the robot; however, mere biped walking on the ground is not sufficient to represent great mobility.

In addition to biped walking, jogging, running, jumping and stair climbing have been also studied for the biped robots as good challengeable topics. M. Gienger et al. of Technical University of Munich in Germany developed their biped humanoid robot, Jogging JOHNNIE with 1.80 m height and 40 kg weight [6]. Its control system was composed of global gait coordination, trajectory generation, and control of the system dynamics. The global gait coordination generated the several prescribed phases of the jogging or walking. In each phase, the prescribed variables were controlled. The trajectory of each phase was generated in the trajectory generation layer. Finally, the robot was controlled by a feedback linearization system to achieve the stabilization. This type of the walking strategy is similar with the strategy of this paper. However, differences are they didn't directly control the ZMP [7] and used the ankle torque control from the feedback linearization during single support phase to maintain the balance. S. Kajita et al. of AIST in Japan developed a HRP-2LR which was able to run in 2005 [8]. The running pattern was calculated by resolved momentum control in offline and the running controller that was composed of body posture control, inverted pendulum stabilization, contact torque control, impact absorbing control, foot vertical force control, and torque distributed controller maintained the balance. By using an inverted pendulum model, they generated reference ankle torques and controlled them to maintain the balance in the joint position control system. Our strategy also uses a similar strategy. However, we designed ZMP compensators to control the ZMP directly for the balance by using not the inverted pendulum model but experimental frequency response test. J. K. Hodgins et al. developed a planar biped jumping robot that can run on rough terrain including the stairs [9]. Its strategy was to adjust step length by controlling forward speed, jumping height, and duration of ground contact by using hydraulic actuators and air springs. The strategy of this robot was different from the typical strategies of recent biped humanoid robots because it didn't have the foot for controlling the ZMP or ankle torques and it used a tether boom for planar motions.

In the case of the stair climbing, we may divide it into static stair climbing and dynamic stair climbing. Generally, static stair climbing consumes over 5 s per step, and dynamic stair climbing has a speed of about 2 s per step. The majority

of the previous works on stair climbing primarily addressed static stair climbing, or dynamic simulations [10–17]. G. Figliolini et al. of University of Cassino in Italy have developed the EP-WAR series. EP-WAR3 was able to going upstairs and downstairs slowly. It walked according to several prescribed phase using a leg mechanism actuated by five double acting pneumatic cylinders, and was also able to maintain the balance by using the two suction-cups on the underside of each foot. The suction-cup technique is their novel method that is different from other researches including us, but the floor must be flat enough. A. Takanishi et al. of Waseda University in Japan developed a biped locomotor WL-16RII using the parallel mechanism that carries a human. It was able to slowly walk on stairs with approximately 6 s of a step time. They minimized the maximum stroke of the linear actuator by tuning up the waist yaw trajectory and derived the walking pattern by tuning up the preset ZMP trajectory in single support phase. It successfully carried a human with 60 kg of the weight, but its walking speed was still somewhat slow.

The reason why dynamic stair climbing is not easy to achieve is that additional vertical motions should be added to horizontal motions and the swinging foot must be moved to a more distant and higher position. The total motion is fundamentally complex and the robot must overcome large disturbances while dynamically climbing the stairs. This paper proposes an experimental control algorithm which only uses force/torque sensors installed at ankle joint in order to realize the dynamic stair climbing of a human-sized biped humanoid robot. Several sensory feedback online controllers modify the stair climbing pattern and joint trajectories during the stair climbing. This sensor feedback modification method has been widely utilized in many research groups. S. Kagami et al. also built their sensor feedback adaptation system that is composed of an adjustment of parameters for the trajectory generation, a reactive adaption for the torso horizontal position modification, a landing position and posture, and landing height adaptation, and an absorption of modeling error that compensates the CM position error and the deformations around the hip roll joints [18]. Since the force/torque sensor has been commonly used as the most basic sensory device to measure the ground reaction forces and torques of a sole in biped robotics society, our control algorithm has a merit in that it can be easily employed by many other biped robots. The proposed control strategy is based on our previous control strategy which has been experimentally proven and generalized through implementation to our robot platforms of KHR-2, KHR-3 (HUBO), Albert HUBO, and HUBO FX-1 [19]. The novel points of this paper, compared to the previous control strategy are listed as follows:

1. We newly designed the stair climbing pattern for the KHR-2.
2. We realized the stair walking by using only the force/torque sensors on the feet without any inertial sensor feedbacks.
3. We proposed three modes of the ZMP compensation.
4. We designed the several ZMP compensators such as the fast/slow SSP ZMP compensators and DSP ZMP compensator through the simulations and experiments, and they are switched according to the ZMP and walking pattern.
5. We realized the stair walking without accurate measurement of the stair height. This was possible because we do not use the absolute vertical walking pattern

with respect to the ground but the relative vertical walking pattern with respect to the pelvis center.

6. We adjusted the landing height at every step by using the force/torque sensors on the feet.

Though we assume that the stair configuration is already known, but we believe our control approach would be a good example of the dynamic stair climbing of human-sized biped humanoid robots. This paper is organized as follows: in "Section 2," we briefly introduce our biped humanoid robot KHR-2 including the overall specifications. Section 3 describes the generation of the standard stair climbing pattern. In "Section 4," the real-time balance control algorithm and three online controllers are described with experimental results. In "Section 5," we verify the effectiveness of the online controllers and the performance of the real-time balance control algorithm via experimentation. Finally, "Section 6" concludes the paper with discussion and suggestions for future research.

2 Brief Overview of Biped Humanoid Robot, KHR-2

In 2003, we developed KHR-2, the second version of our biped humanoid robots (Fig. 1). Since it is a human-friendly intelligent robot, we designed it to be the size of a child and gave it sufficient joints to imitate human motions. The height, weight and total number of degrees of freedom of KHR-2 are 56 kg, 120 cm and 41 (six for each leg, four for each arm, seven for each hand, one for torso and six for head) respectively. All joint actuators are brushed DC motors with harmonic reduction gears or planetary gears. We achieved a self-contained system by putting all mechanical and electronic parts into the robot body. Hence, KHR-2 is tele-operated via wireless Local Area Network (LAN). Detailed specifications, DOF, and dimensions are described in Tables 1 and 2.

The control system architecture of KHR-2 is a distributed control system. The main computer is installed in the torso and sub-controllers such as joint motor controllers and sensory devices are distributed throughout the whole body.

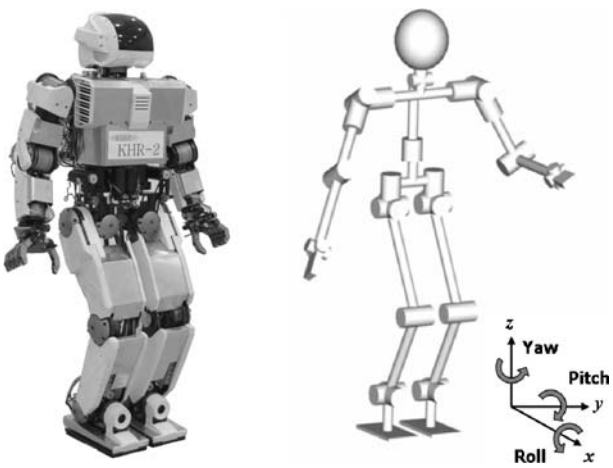

Fig. 1 Biped humanoid robot, KHR-2

Table 1 Specification of humanoid robot, KHR-2

Height	120 cm	
Weight	56 kg	
DOF	41	
Waking speed	0∼1. 25 km/h	
Grasping force	0.5 kg/finger	
Actuator	Brushed DC motor with harmonic drive gear/planetary gear	
Sensory devices	Three-axis force/torque sensors on wrists and feet	
	Two-axis inertial sensor at torso	
	2-axis tilt sensors at feet	
	Stereo color CCD camera	
Power supply	Battery	Ni-MH (24 V/6.6AH,) 12 V/9.9AH
	External Power	12 V, 24 V
Operating device	Laptop PC with wireless LAN	

Communication between the main computer and the sub-controllers is achieved by using Controller Area Network (CAN) protocol (Fig. 2). As for a motion control process, the main computer generates desired motions of end-effectors, calculates desired joint angles using inverse kinematics, and transmits data to all joint motor controllers in real-time, and then each joint motor controller controls the angular position of the joint using encoder feedback (Fig. 3). Here, it is important to note that control rate of the main computer is ten times lower than that of servo controllers. This is for reducing the computing burden of the main computer, so other jobs such as image processing, wireless networking, speaking and so on. can be performed simultaneously.

By using above architecture, we built a fundamental control structure walking control (Fig. 4). Biped walking is composed of the walking pattern planning and the posture stabilization. The walking pattern planning can be thought as a feed-forward control term and the posture stabilization can be thought as a feedback control term.

Table 2 Degrees of freedom and dimensions of KHR-2

Head	Eye (pan and tilt)		2 DOF × 2 = 4 DOF	
	Neck (pan and tilt)		2 DOF	
Arm	Shoulder (roll/pitch/yaw)		3 DOF × 2 = 6 DOF	
	Elbow (pitch)		1 DOF × 2 = 2 DOF	
Hand	Wrist (roll/pitch)		2 DOF × 2 = 4 DOF	
	Finger		1 DOF × 5 × 2 = 10 DOF	
Torso	Waist (yaw)		1 DOF	
Leg	Hip (roll/pitch/yaw)		3 DOF × 2 = 6 DOF	
	Knee (pitch)		1 DOF × 2 = 2 DOF	
	Ankle (roll/pitch)		2 DOF × 2 = 4 DOF	
Total			41 DOF	
Dimensions (mm)	Height	1,200	Length of upper leg	290
	Width (shoulder to shoulder)	420	Length of lower leg	280
	Depth (chest to back)	213	Length between hip joint s	142
	Length of upper arm	184	Width of sole	140
	Length of lower arm	185.5	Length of sole	233

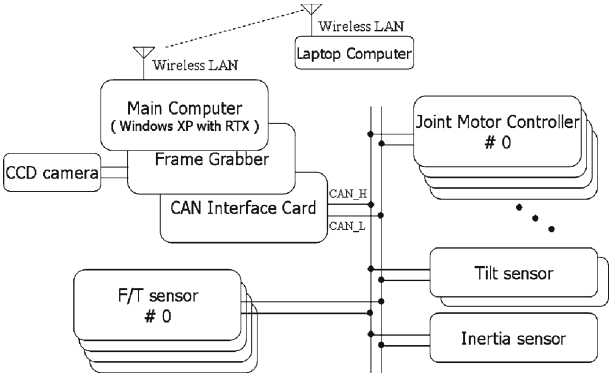

Fig. 2 Overall system configuration of KHR-2

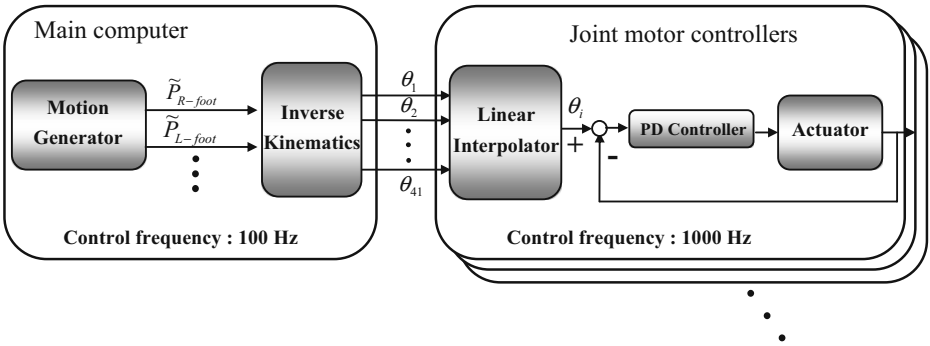

Fig. 3 Motion control process of KHR-2

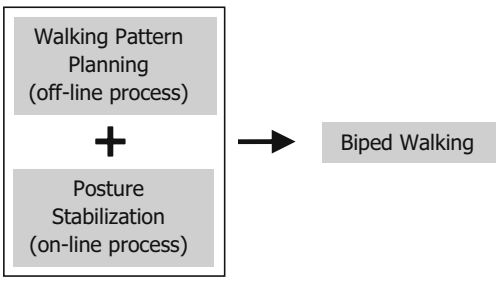

Fig. 4 Fundamental control structure of biped walking

3 Stair Climbing Pattern

To achieve human-like dynamic stair climbing, a suitable walking pattern is needed because our motion control strategy is fundamentally based on the position control of joints. In the case of stair climbing, the elevation and step length of the swing foot are larger than those of other walking patterns because the swinging foot has to be moved onto the surface of the stair. Hence, basically, we always carefully considered the required angular velocity, torque of each joint, the maximum RPM of the DC motor, and the reduction gear ratio. We designed the standard stair climbing pattern by considering the following factors as well as the stair configuration.

3.1 Stair Climbing Ready Pose

KHR-2 lowers its pelvis 40 mm at a full straight legged pose during stair climbing in order to make bent-knee pose and prevent the singularity problem in calculating inverse kinematics (Fig. 5). In our previous works on dynamic biped walking on the ground [19], we set the walking period (stride time) to 1.9 s by using the natural frequency of the 2D pendulum model shown in following Eq. 1 below because the l is about 0.9 m when KHR-2 lowers its height 40 mm. This means that the pelvis height is related to the walking period.

$$f = \frac{1}{2\pi}\sqrt{\frac{g}{l}}\ (\mathrm{Hz}) \tag{1}$$

where, g and l are the gravitational acceleration and height of the mass center of the robot from the ground. In this manner, energy during walking can be efficiently consumed because a little swing motion generates sufficiently large movement. On the other hand, in the case of a stair climbing pattern, we set the walking period to about two times longer than that of forward walking on normal floor. We think

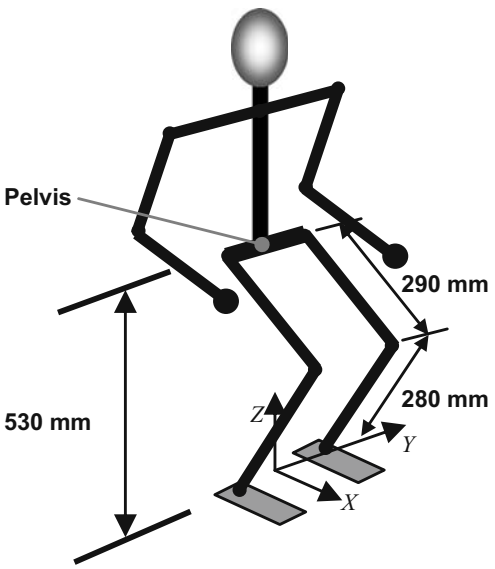

Fig. 5 Stair climbing ready pose

that Eq. 1 also can be applied to a walking period of a stair climbing, but we had to consider the speed limit of the knee motor. Therefore, we ignore Eq. 1 for a stair climbing pattern and maintain the same lowering distance of the pelvis in spite of the large energy consumption.

3.2 Essential Factors

To generate a stair climbing pattern, the following essential factors should be considered [20]. For a reference, a walking cycle is described in Fig. 6.

1. Walking period (Stride time, stride time = step time × 2)
2. Double support ratio: portion of double support phase in a walking cycle
3. Lateral swing amplitude of pelvis

By considering the dimensions of an ordinary stair, we determined the walking period to be 4.4 s so that KHR-2 can sufficiently step forward over 250 mm with a foot elevation of over 150 mm sufficiently in a step time. The double support ratio is a percentage of the double support phase in a walking cycle. In the case of humans, the double support ratio is more than 10% [20]. For KHR-2, we experimentally set this value to 5% because KHR-2 does not have toe joints that can lengthen the double support phase easily. Next, the lateral swing amplitude of pelvis was determined to be 65 mm according to ZMP dynamics of simple inverted pendulum. This value is about two times larger than that of forward walking on normal floor because the walking speed of stair climbing is slower. The inertial force caused by the lateral acceleration is become small, so larger swing amplitude is needed to shift ZMP to each foot. Following ZMP dynamic equation of a 2D simple inverted pendulum clearly demonstrates the above explanation

$$Y_{zmp} = Y_{mc} - \frac{l}{g}\ddot{Y}_{mc} \tag{2}$$

where, Y_{mc} is the lateral displacement of mass center, l is the height of mass center from the ground, Y_{zmp} is the lateral component of ZMP and g is the gravitational

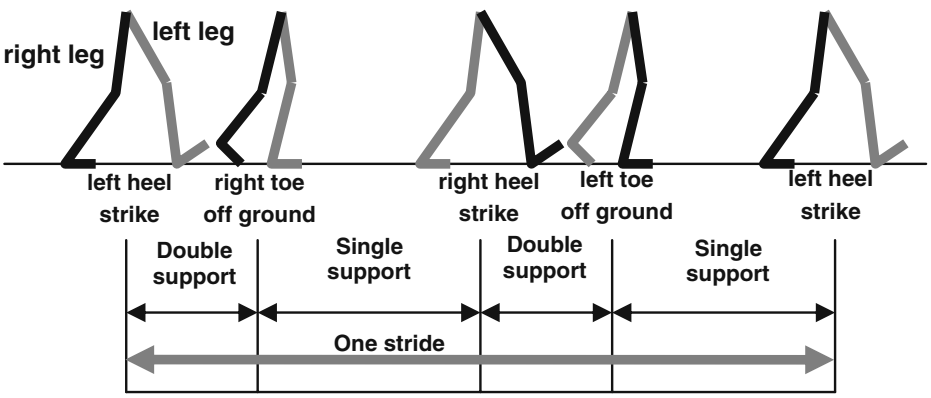

Fig. 6 Walking cycle

acceleration respectively. If we assume the lateral displacement of the mass center as $Y_{mc} = A\sin\omega t$, we obtain,

$$Y_{zmp} = A\left(1 + \frac{l}{g}\omega^2\right)\sin\omega t. \tag{3}$$

In Eq. 3, if the walking frequency, becomes higher due to fast walking, even small pelvis lateral swing, A can easily shift the ZMP to each center of sole. On the contrary, if the walking speed is lowered, large lateral swing amplitude of the pelvis is necessary. For the stair climbing, since the walking frequency and l are 1.428 rad per second and 0.9 m, the Eq. 3 becomes following equation.

$$Y_{zmp} = 1.187A\sin\omega t. \tag{4}$$

Since desired lateral ZMP amplitude is 77 mm, so the lateral swing amplitude of pelvis, A should be about 65 mm. 77 mm of the desired lateral ZMP amplitude was determined considering the distance between the foot center and the pelvis center is 71 mm.

3.3 Stair Climbing Pattern Design

Before generating the stair climbing pattern, we built two coordinate frames. The body fixed coordinate frame is attached in the pelvis center, so it is used for the indication of the relative positions of the two feet from the pelvis. The ground fixed coordinate indicates the absolute positions of the pelvis and the two feet from a specific point on the ground. The coordinate frames and the configuration of the stair are shown in Fig. 7.

In accordance with three essential factors, we designed trajectories for the pelvis and two feet (Fig. 8). For the pelvis, an absolute lateral (Y-dir.) trajectory with

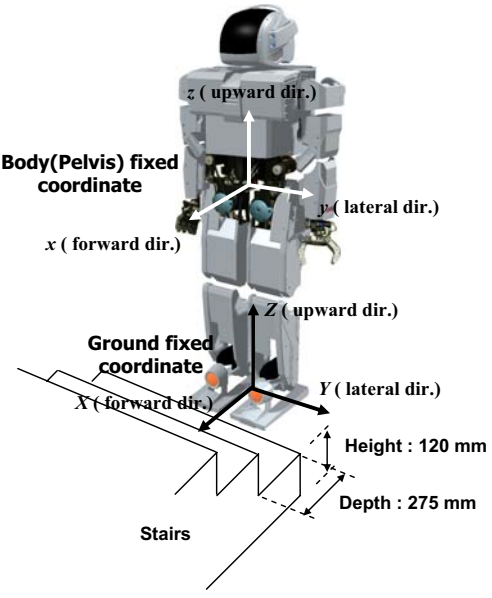

Fig. 7 The coordinate frames of KHR-2 and the stair configuration

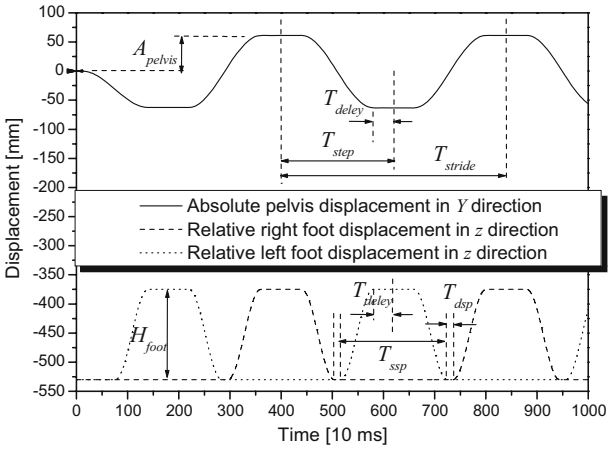

Fig. 8 Stair climbing pattern

respect to the ground-fixed coordinate was designed by using the cosine function in order to produce a smooth curve and also to eliminate the velocity discontinuity. The step time is 2.2 s and the swing amplitude is 65 mm. For the two feet, each foot requires relative vertical ($z-$dir.) movement. The maximum elevation of the foot is 155 mm and its relative vertical trajectory with respect to the body-fixed coordinate was also generated by using the cosine function. The reason why we did not draw absolute vertical trajectories of the two feet is that we do not know the actual height of the stair in reality. Since we determined the maximum elevation of the foot as 155 mm, KHR-2 can climb a variable stair height up to 155 mm ideally. The dimensions of the stair climbing pattern are written in Table 3. The delay time, T_{delay} near the peak portions of the pelvis and feet trajectories is for the fast ZMP switching to each sole by reducing transition period.

Next, the stair climbing pattern is completed by adding the relative forward (x-dir.) trajectories of the two feet with respect to the body fixed coordinate. Firstly, we designed absolute forward (X-dir.) trajectories of the two feet and pelvis, and then converted them into the relative forward trajectories of the two feet. As for an absolute trajectory of the pelvis in a forward direction, an absolute pelvis trajectory was generated by mixing the cosine and straight line functions with an appropriate ratio. Since the depth of a stair is 275 mm, the pelvis has to move forward 275 mm during a step time. Hence, we set the step length L_{step} to 275 mm. As for the absolute

Table 3 The design parameter of stair climbing pattern

	Description	Value
A_{pelvis}	Lateral swing amplitude of pelvis	65 (mm)
H_{foot}	Maximum elevation of foot	155 (mm)
L_{step}	Step length (stride / 2)	275 (mm)
T_{stride}	Walking period (stride time)	4.4 (s)
T_{step}	Step time	2.2 (s)
T_{delay}	Delay time	0.4 (s)
κ_{dsp}	Double support ratio	0.05 (5%)
T_{ssp}	Single support time	$T_{step} \times (1.0 - \kappa_{dsp})$
T_{dsp}	Double support time	$T_{step} \times \kappa_{dsp}$

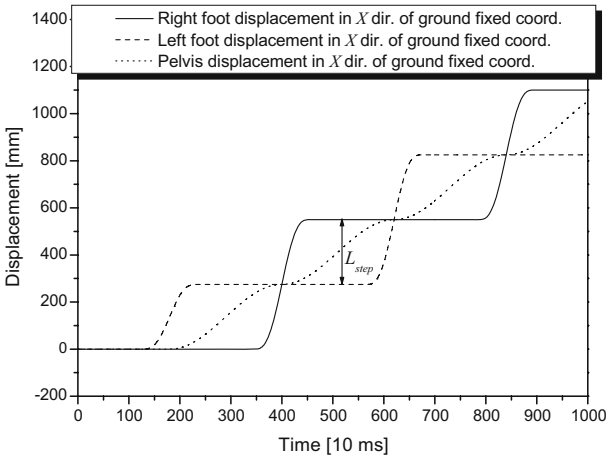

Fig. 9 Absolute feet and pelvis trajectories in X dir. of stair climbing (step length: 275 mm)

trajectories of the two feet in a forward direction, we used a cycloid function. The reason why we chose this function for the foot trajectory is that the human ankle is circling the tiptoe while walking. Likewise, the cycloid function describes a path of a certain point on the circumference of a circle during circling. All forward trajectories are plotted in Fig. 9. Finally, the relative trajectories of the two feet are derived by following relationships.

$$\text{Relative foot trajectory} = \text{Absolute foot trajectory} - \text{Absolute pelvis trajectory} \tag{5}$$

Relative trajectories of the two feet are also shown in Fig. 10.

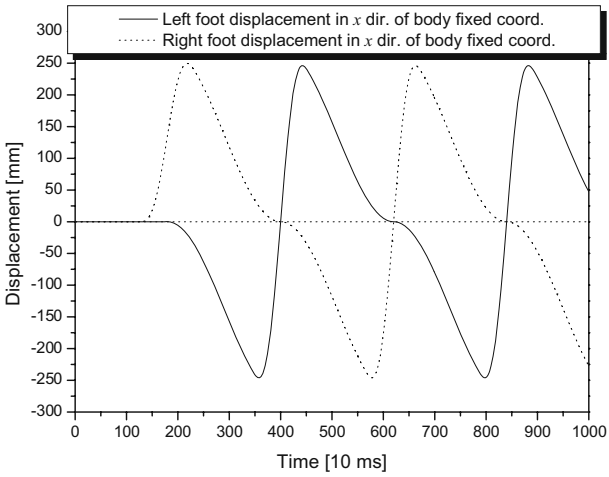

Fig. 10 Relative feet trajectories in x dir. of stair climbing (step length: 275 mm)

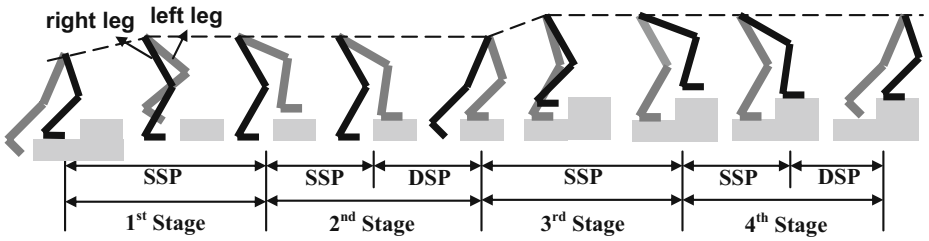

Fig. 11 Stair climbing stages during one walking cycle

4 Real-Time Balance Control Scheme

In our previous work, we explained that online dynamic walking control is composed of three kinds of the control schemes: real-time balance control, walking pattern control and predicted motion control [19]. In this research, we only apply the real-time balance control scheme because the real-time stability is the most important factor for dynamic stair climbing.

4.1 Stair Climbing Stages

We defined five stair climbing stages according to the various climbing motions because a robot's dynamic characteristic of the each stage is different. By dividing the stages during a walking cycle, we can predict the climbing situations easily and plan proper balance control strategies. The stages 1–4 are repeated during stair climbing. Stage 5 is the standstill pose after the robot finishes climbing the stairs. These stages are described below corresponding to Fig. 11:

1. First stage: continue to lower the right foot to the prescribed height from the pelvis center and lift the left leg to its prescribed height from the pelvis center.
2. Second stage: lower the left leg until it makes complete contact with the stair, and then hold the lowering of the left leg until the starting of the next stage (third stage).
3. Third stage: continue to low the left foot to the prescribed height from the pelvis center and lift the right leg to its prescribed height from the pelvis center.
4. Fourth stage: lower the right leg until it makes complete contact with the stair, and then hold the lowering of the right leg until the next stage (first state).
5. Fifth stage: after completing stage 1 or 3, brings the robot to a stop pose with both legs planted firmly on the stair.

4.2 Overview of Control Strategy

The real-time balance control scheme is composed of three online controllers; the damping controller, ZMP compensator, and landing controller. Each controller is activated in certain stages for dynamic stable climbing. Table 4 shows the time schedule of the online controllers. All online controllers will be explained in detail.

Table 4 Time schedule of online controllers

Control Scheme	Online Controller	1st stage	2nd stage		3rd stage	4th stage		5th stage
			S	D		S	D	
Real-Time Balance Control	Damping Controller	■	■		■	■		
	SSP ZMP Compensator	■	■		■	■		
	DSP ZMP Compensator			■			■	■
	Landing Controller	■		■	■		■	

Grey box: controller is at work

S single support phase, *D* double support phase

4.3 Damping Controller

The damping controller was designed to eliminate the sustained structural oscillation in the single support phase during stair climbing [21]. This oscillation is mainly caused by a high-gained joint position control and the force/torque sensor that is installed on the ankle joints as a part of compliant structure. Hence, we modeled the robot as a simple inverted pendulum with a compliant joint and designed the damping controllers in order to impose sufficient damping forces in ankle rolling and pitching joints without changing the steady state value. Figures 12 and 13 show the mathematical modeling and control block diagram respectively. In Fig. 12, l is the distance from the ground to the mass center, m is total point mass, u is the reference joint angle, is the actual joint angle due to the compliance, K is the spring constant, T is the measured torque, and g is the gravitational acceleration respectively. Then, the equation of motion can be written as follows:

$$T = mgl\theta - ml^2\ddot{\theta} = K(\theta - u). \tag{6}$$

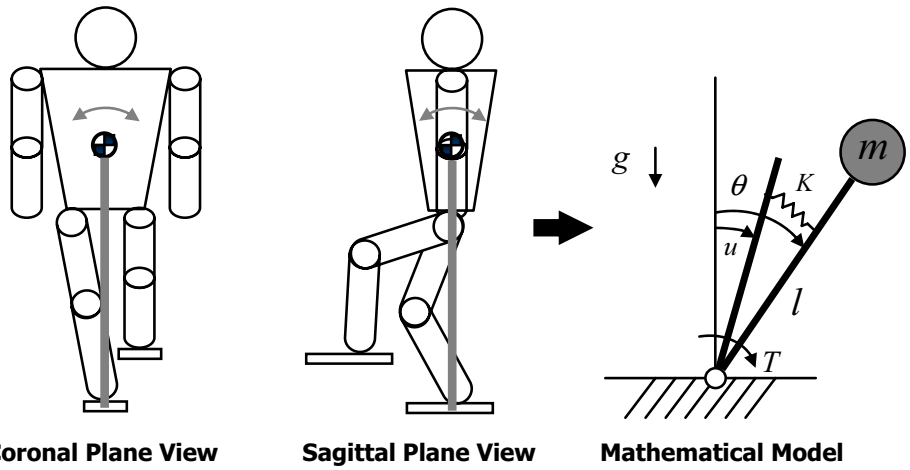

Fig. 12 Inverted pendulum model with a compliant joint in the single support phase

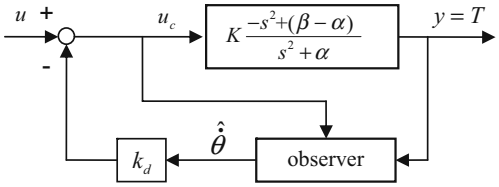

Fig. 13 Block diagram of the damping control

From, above equation, we can obtain transfer function from the reference joint angle to the measured torque.

$$\frac{T}{u} = K\frac{-s^2 + (\beta - \alpha)}{s^2 + \alpha} \tag{7}$$

where,

$$\alpha = \frac{K}{ml^2} - \frac{g}{l} > 0\,, \quad \beta = \frac{K}{ml^2}$$

In Eq. 7, the unknown parameters are l and K. These parameters can be identified by free response and steady state experiments. In other words, by measuring the oscillation period and steady state value of the torque from unity input, we can derive the unknown values easily. This system has two poles which are nearby the imaginary axis, so the system shows the characteristics of a lightly damped system. To suppress the oscillation, more damping force is necessary for the ankle joints. Therefore, the damping control law is designed as follows:

$$u_c = u - k_d\hat{\dot{\theta}}. \tag{8}$$

where, k_d is a damping control gain, u_c is a compensated joint angle and $\hat{\dot{\theta}}$ is an observed angular velocity of the joint respectively. In the equation above, $\hat{\dot{\theta}}$ is derived by following observer equation.

$$\dot{w} = -L_o w - \left(L_o^2 + \alpha\right)(y + Ku_c) + K\beta u_c \tag{9}$$

$$\hat{\dot{\theta}} = \frac{1}{K}w + \frac{L_o}{K}(y + Ku_c) \tag{10}$$

where, L_o is the pole of the observer. As the observability matrix has a full rank and a typical Luenburger observer was used, the observed state definitely converged to the actual state. We first set the observer gain close to the -4.0 in the Laplace domain in order that the settling time becomes about 1 s for the second order system. By trial and error of the Matlab simulation, we were able to tune the observer gain that follows the actual angular position and velocity well, and the feedback gain k_d. Finally, we retuned the observer gain and feedback gain through experiments. As for the experiment, we gave external forces to the robot in the single support phase, and then check the ankle torque response. The damping controller is applied to the rolling and pitching joints of ankles. Figures 13 and 14 show control block diagram and the experiments of the damping controller respectively. It is obvious that the oscillations of the moments are quickly eliminated by applying the damping control. Therefore, the robot can walk without oscillations of the body.

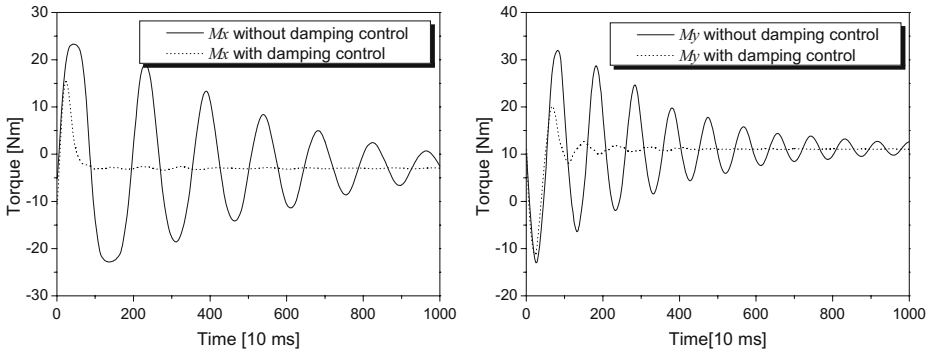

Fig. 14 Experimental results of damping control during the single support phase

4.4 ZMP Compensator

ZMP has played an important role in the stable walking of biped humanoid robots [7]. This is because it is easy to measure ZMP by means of a force/torque sensor at ankle joint or pressure sensor on the sole. Besides, ZMP gives a definite stability criterion. Though ZMP is only measured in the presence of contact between foot and the ground and may be incorrect on an uneven and tilted ground surface, its utility is quite well known to many researchers. Most researchers in the field of biped robotics have studied about ZMP control for biped humanoid robots.

In this paper, we designed ZMP compensators in the single support phase and the double support phase because the damping controller is working in the only single support phase and it alone would not suffice to maintain stable walking. More specifically, the damping controller only eliminates the large ankle torque oscillations in the single support phase by giving the damping force at the ankle joint. Therefore, the damping controller alone cannot regulate the ZMP and allows the steady state ZMP error. In other words, the damping controller cannot guarantee the stable walking. However it can enhance the walking stability by eliminating the oscillations. For this reason, we additionally designed the ZMP compensators for the ZMP regulation after we developed the damping controller.

To compensate for ZMP error, we divided the ZMP compensation strategy into three modes because the dynamics is quite different according to the robot's different poses. Then, we decided to use the horizontal motion of the pelvis. That is, absolute pelvis displacement (X_{pelvis}, Y_{pelvis}) on the transverse plane were used as a control input (Fig. 15). We designed various ZMP compensators for the three modes as follows:

1. Mode 1: DSP ZMP compensator of mode 1
2. Mode 2: DSP ZMP compensator of mode 2
3. Mode 3: SSP ZMP compensator

As for mode 1, two feet are aligned in the double support phase. This mode is for the stabilization of standstill of the robot. In other words, before or after climbing stairs, the DSP ZMP compensator of mode 1 stabilizes the robot. As for mode 2, two feet are placed apart from each other in a forward direction in the double support

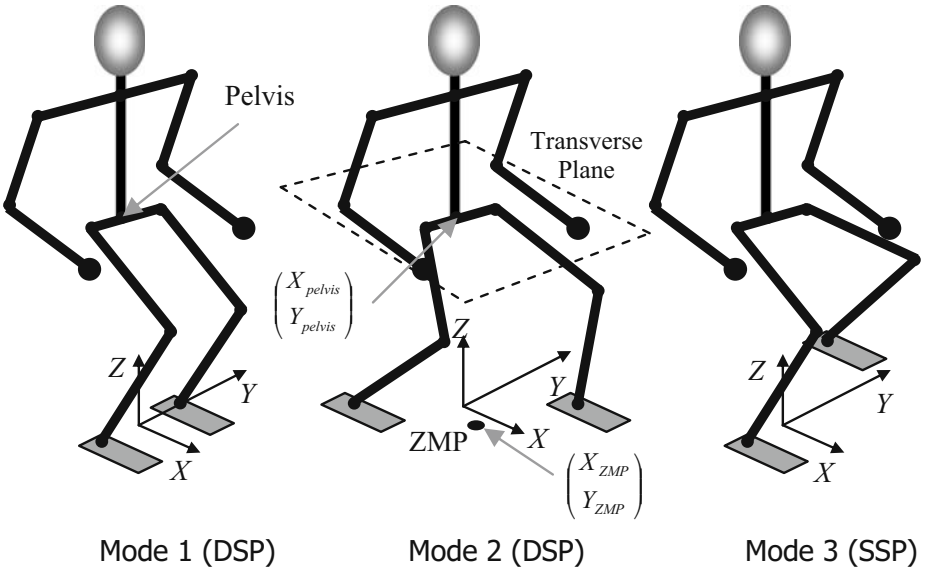

Fig. 15 ZMP compensation modes

phase. This mode occurs for the periods of double support phase of the second stage or fourth stage. In this mode, DSP ZMP compensator of mode 2 is applied to maintain the stability during going upstairs. In reality, the foot positions in vertical direction of both feet are not the same, and a distance between two feet in forward direction is also changeable. Therefore, we derived a suitable ZMP compensator on ground with a 200 mm of distance between two feet in forward direction, and then experimentally tuned the control gains again through stair climbing experiments. As for mode 3, this mode is completely in the single support phase because one foot is lifted from the ground. This mode arises from the start of the first stage to the end of SSP of the second stage or from the start of the third stage to the end of SSP of the fourth stage. In this mode, the SSP ZMP compensator also stabilizes the robot in spite of the large swing and lifting motion of foot. All ZMP compensators of the three modes are designed in the same way, so we present the DSP ZMP compensator of mode 1 and the SSP ZMP compensator in this paper.

4.4.1 DSP ZMP Compensator of Mode 1

At the end of stair climbing, the biped humanoid robot will be in the double support phase. The moment the robot puts its lifted foot back on the floor, the robot is apt to be oscillated in the pitching and rolling directions unless it controls its attitude. This oscillation may cause falling down toward the pitching or rolling direction. It is necessary to stabilize the robot against the oscillation during the double support phase. From this point of view, we determined to compensate the forward component, X_{ZMP} and the lateral component, Y_{ZMP} of ZMP by moving the pelvis in forward and lateral directions on the transverse plane. Firstly, we derived the transfer functions in forward and lateral directions by experimental frequency response analysis. We gave the sinusoidal pelvis displacement in the

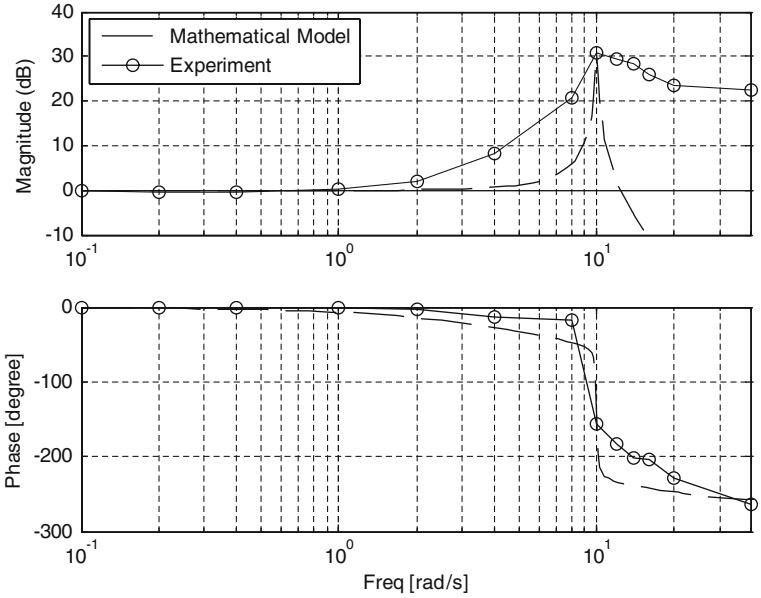

Fig. 16 Bode plot of transfer function Y_{ZMP}/Y_{pelvis} of mode 1

ground fixed coordinate frame, and then collected ZMP. From Figs. 16 and 17 of the experimental results, at the frequency of 10 rad/s and the phase of −180°, the magnitudes have the peak values. Furthermore, the phase angles converge to

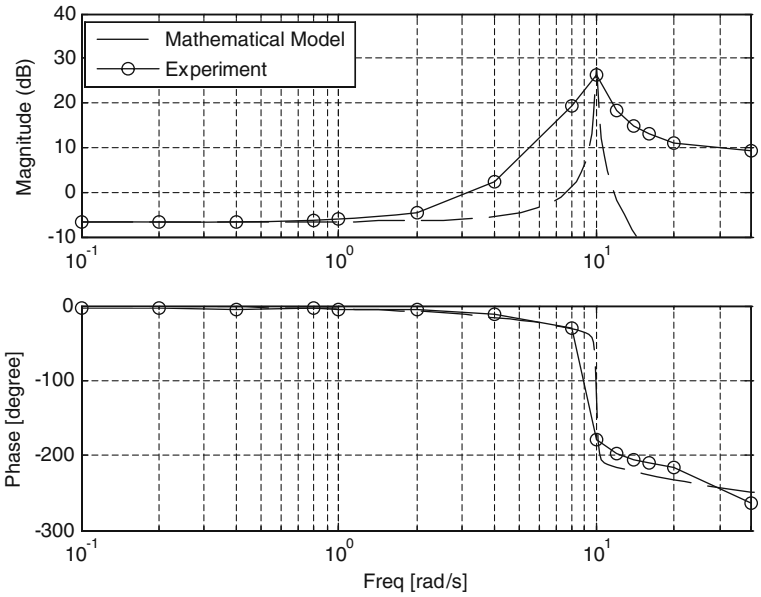

Fig. 17 Bode plot of transfer function X_{ZMP}/X_{pelvis} of mode 1

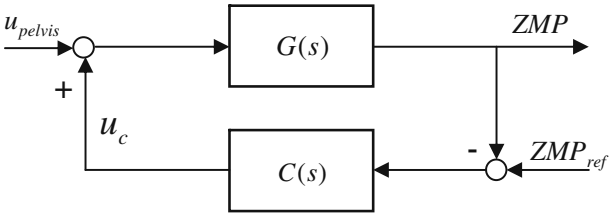

Fig. 18 ZMP compensation block diagram

$-270°$ at high frequency. Therefore, it becomes clear that these transfer functions are third order and type 0 systems. The second and third coefficients of the second order polynomial in the denominator of the transfer function were derived by the magnitude value and the frequency at the resonance. One more pole in the transfer function was derived by the phase curve shape. Also, the gain in the nominator of the transfer function was derived by the magnitude in the low frequency. Finally, we mathematically modeled each system as a simple third order system as follows:

$$\frac{Y_{ZMP}}{Y_{pelvis}} = G_Y(s) = \frac{800.128}{\left(s^2 + 0.18s + 100.016\right)(s+8)} \tag{11}$$

$$\frac{X_{ZMP}}{X_{pelvis}} = G_X(s) = \frac{697.65}{\left(s^2 + 0.156s + 100.012\right)(s+15)} \tag{12}$$

Next, we designed the ZMP compensators in mode 1 by using the pole placement technique [22]. Figure 18 shows a feedback diagram in which ZMP_{ref} is the reference ZMP, C(s) is the compensator, and G(s) is the transfer function. u_{pelvis} and u_c are the displacement of prescribed trajectory and the compensatory displacement of the pelvis on transverse plane in the ground fixed coordinate frame respectively. Consequently, the pelvis displacements from the standard stair climbing pattern and the compensator are superimposed in real-time. To realize the arbitrary pole assignment, we determined to design fourth order compensators. Figure 19 shows the system poles, closed-loop poles, controller poles and zeros of forward direction. Since

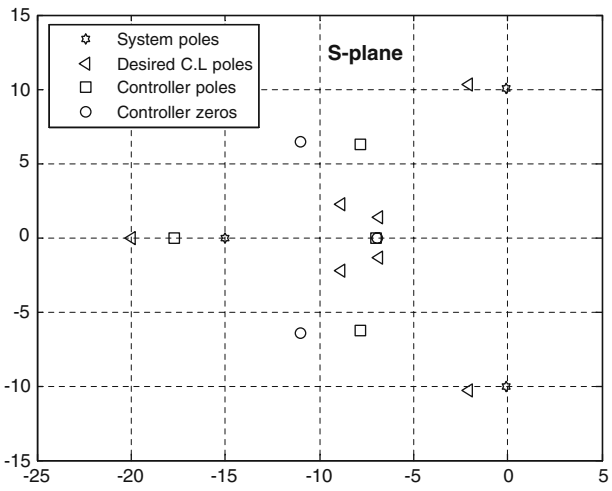

Fig. 19 DSP X_{ZMP} controller design of mode 1 using the pole placement technique

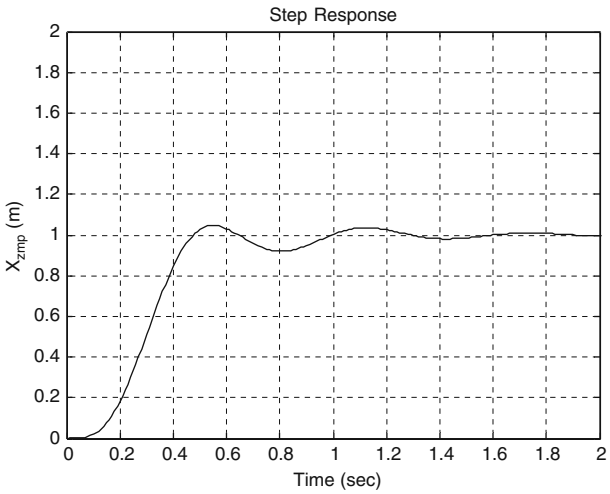

Fig. 20 Step response of the DSP X_{ZMP} compensator of mode 1

the many closed-loop poles should be required to be positioned, the Butterworth pole configuration was used first. And then, we adjusted the positions of the closed loop poles by using Matlab simulations and experiments. Actually, for the arbitrary pole placement, the minimum order of the compensator is two. However, we intentionally attached a predefined pole in the compensator for the smooth output signal, hence the order of the compensator became four. In this manner, the DSP X_{ZMP} compensator and Y_{ZMP} compensator of mode 1 are written as follows:

$$C_X(s) = \frac{-185.34s^3 - 5367.7s^2 - 58501.01s - 209477.1}{15s^4 + 606.27s^3 + 9188.94s^2 + 66455.8s + 186868.04} \tag{13}$$

$$C_Y(s) = \frac{-15.79s^3 - 740.66s^2 - 9071.7s - 31953.44}{8s^4 + 340.83s^3 + 5248.63s^2 + 38158.76s + 107625.5} \tag{14}$$

The step response simulation of the above DSP X_{ZMP} compensator was shown in Fig. 20, and its ZMP regulation performance was also checked experimentally in Fig. 21. To derive the compensator, the rough closed loop pole locations were defined by using the step response Matlab simulations. And then the ZMP regulation experiments under the large external disturbance were conducted in order to precisely tune the locations of the closed loop poles. When we applied disturbance to the robot in forward and lateral directions, it was observed that the ZMP oscillation was eliminated quickly. Therefore, the DSP ZMP compensator of mode 1 successfully maintained the stability against the disturbances during the double support phase. The same strategy was also applied to the DSP ZMP compensator of mode 2.

4.4.2 SSP ZMP Compensator

During stair climbing, it is most important to stabilize the robot in the single support phase. This is because the period is long, and the lift and swing motions of the foot are so large in comparison with biped walking on the ground. The SSP ZMP compensator also was designed in the same way that we designed the DSP ZMP compensator of mode 1. Moreover, we developed two kinds of SSP ZMP compensators which have

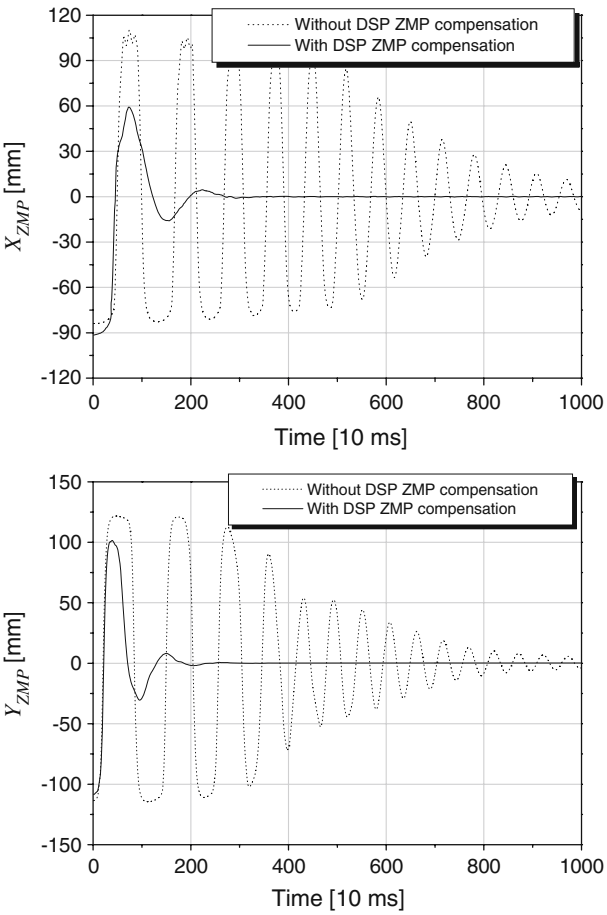

Fig. 21 ZMP regulation experiments of DSP ZMP compensator of mode 1

different characteristics from each other. One has a characteristic of a PD controller and the other acts like a PI controller. These controllers are used together according to the stability boundaries that we defined.

To derive transfer functions, we also carried out frequency response experiments in the presence of the damping control because the damping control is applied at all times during the single support phase. As shown in Figs. 22 and 23, at a frequency of 10 rad/sec and a phase of −180 degrees, the magnitudes reach their peak values, and the phase angles converge to −360° at high frequency. Hence, we can assume transfer functions are fourth order and type 0 systems simply. Here, we proposed a transfer function that is a square of the second order system as one of the simplest mathematical models. By using the same procedure in the DSP ZMP compensator of mode 1, we mathematically modeled the transfer functions as follows:

$$\frac{X_{ZMP}}{X_{pelvis}} = G_X(s) = \frac{6668.34}{\left(s^2 + 3.68s + 106.77\right)^2} \tag{15}$$

$$\frac{Y_{ZMP}}{Y_{pelvis}} = G_Y(s) = \frac{28541.65}{\left(s^2 + 4.59s + 131.52\right)^2} \tag{16}$$

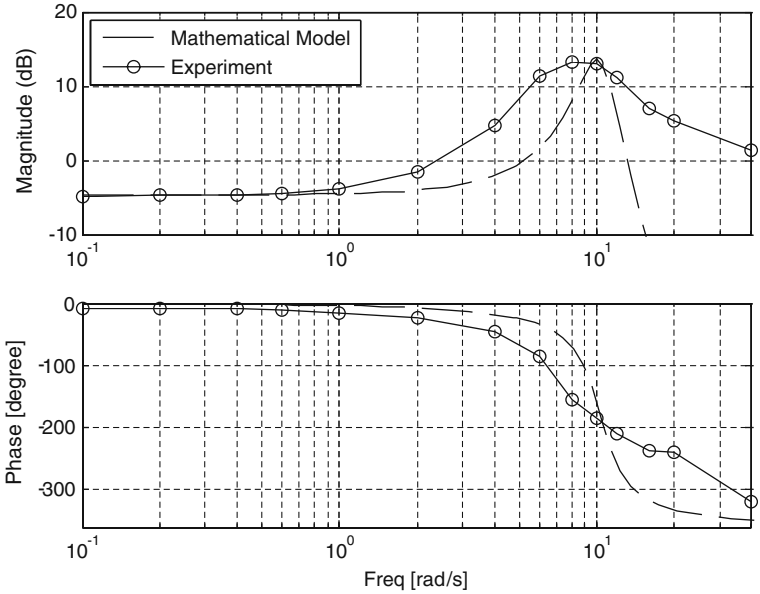

Fig. 22 Bode plot of transfer function X_{ZMP}/X_{pelvis} of the single support phase

We also designed fifth order SSP ZMP compensators by using the pole placement technique. In SSP compensator design, each compensator has an integrator, $1/(s+\alpha)$ (α is a positive real number), which helps to prevent steady state error

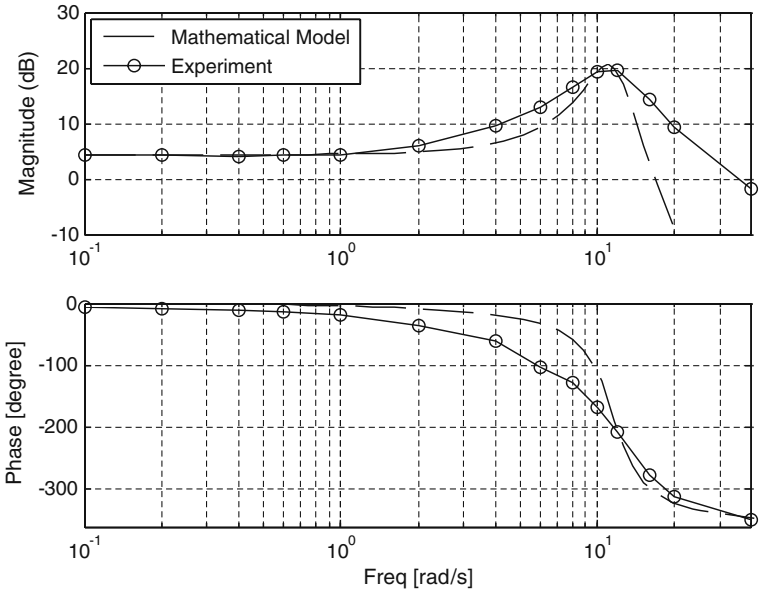

Fig. 23 Bode plot of transfer function Y_{ZMP}/Y_{pelvis} of the single support phase

and improves the continuity of the control input. If we define α as a positive small number, the compensator will have the characteristics of a PI controller. From now on, we will call this kind of compensator a slow SSP compensator. On the contrary, if we define α as a positive large number, the compensator behaves like a PD controller. We will call this compensator a fast SSP compensator. After the same design procedure represented in the DSP ZMP compensator of mode 1, the fast and slow SSP ZMP compensators were designed as follows:

$$C_X^{fast}(s) = \frac{-62.065s^4 - 3020.8s^3 - 35673.5s^2 - 355565.5s - 1196033.3}{s^5 + 70.44s^4 + 2255.6s^3 + 40240.4s^2 + 376617.8s + 1118129.2} \tag{17}$$

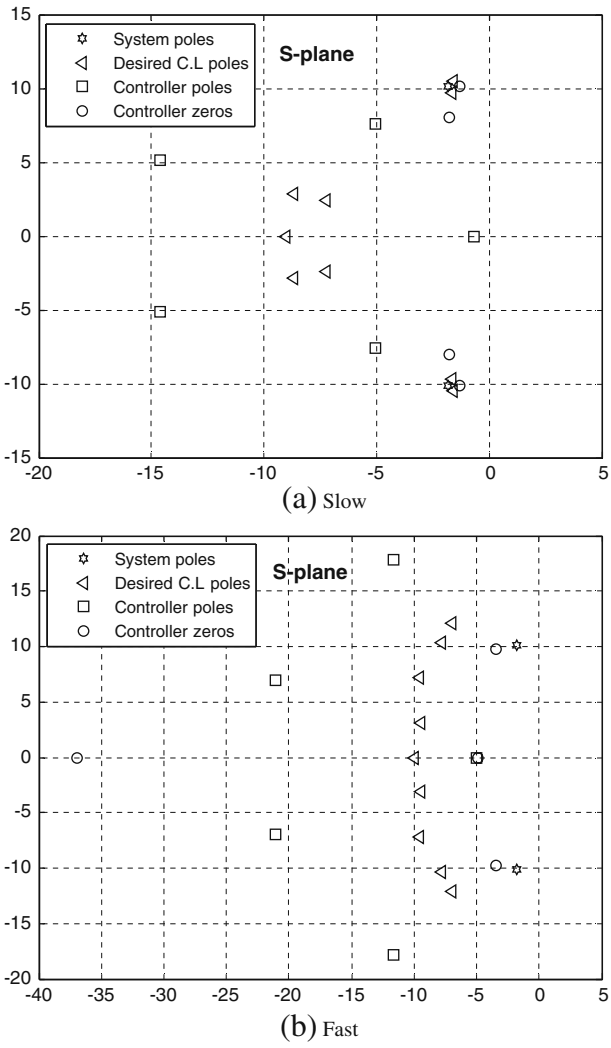

Fig. 24 Slow and fast SSP X_{zmp} compensator designs using the pole placement technique

$$C_Y^{fast}(s) = \frac{-34.97s^4 - 1396s^3 - 18287.5s^2 - 185137.6s - 607515.1}{s^5 + 80s^4 + 2831.7s^3 + 54573.2s^2 + 530148.6s + 1593487.3} \tag{18}$$

$$C_X^{slow}(s) = \frac{6.7s^4 + 41.36s^3 + 1220.45s^2 + 3701.25s + 47755.66}{s^5 + 39.96s^4 + 644.63s^3 + 5279.9s^2 + 23365.4s + 13980.36} \tag{19}$$

$$C_Y^{slow}(s) = \frac{3.56s^4 + 10.81s^3 + 678.08s^2 + 522.5s + 28379.35}{s^5 + 43.05s^4 + 761.27s^3 + 7209.6s^2 + 42172.8s + 35682.4} \tag{20}$$

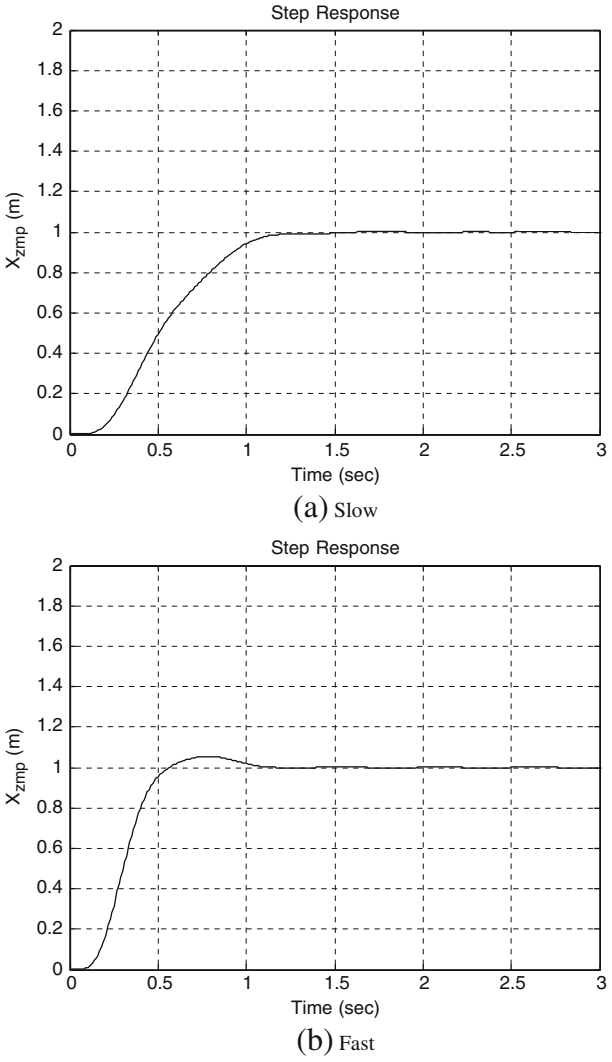

Fig. 25 Step response of the slow and fast SSP X_{zmp} compensators

Figures 24 and 25 show a compensator design using the pole placement and the simulation results of the step response. To verify the performance of the SSP ZMP compensators, we carried out several experiments. When we applied external disturbances to the robot during the single support phase, we observed the responses of the robot. Firstly, we compared the case of no control with the case of the damping control. In Fig. 26, it is seen that ZMP oscillations are reduced rapidly by the damping control, but there are small ripples, large overshoots and steady state errors. Here, in the ZMP compensation, reference X_{ZMP} is 10.0 mm and reference Y_{ZMP} is -80.0 mm respectively. These ripples can be eliminated and overshoots are reduced by fast SSP ZMP compensators (Fig. 27). By the way, fast SSP ZMP compensators still cannot eliminate steady state errors because the compensators have little integral control action. To remove steady state errors, we applied slow SSP ZMP compensators. These slow SSP ZMP compensators can eliminate steady state errors by using integral control action but, large overshoots and small ripples appear again (Fig. 28). Therefore, we tried to apply fast SSP ZMP compensator and

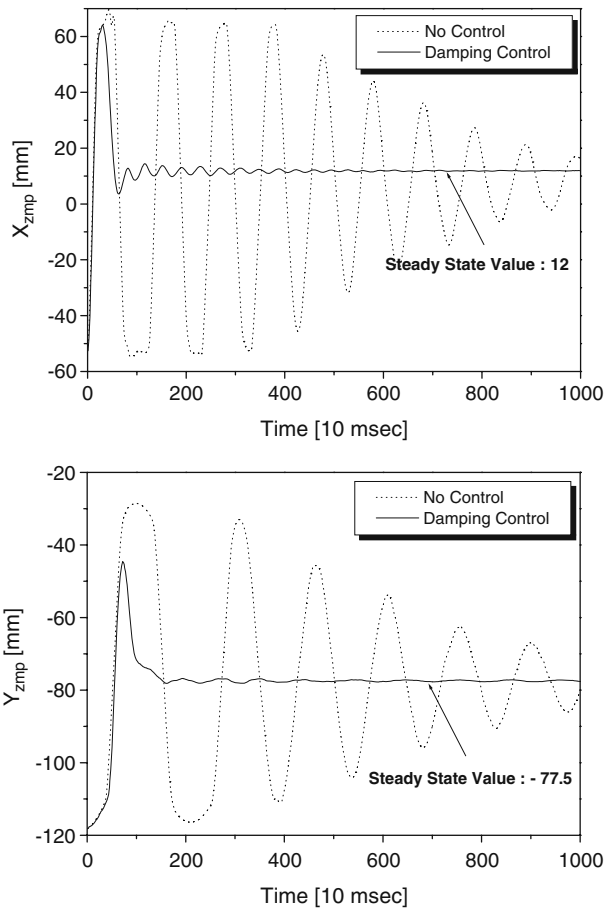

Fig. 26 A ZMP regulation comparison between the case of no control and the case of damping control

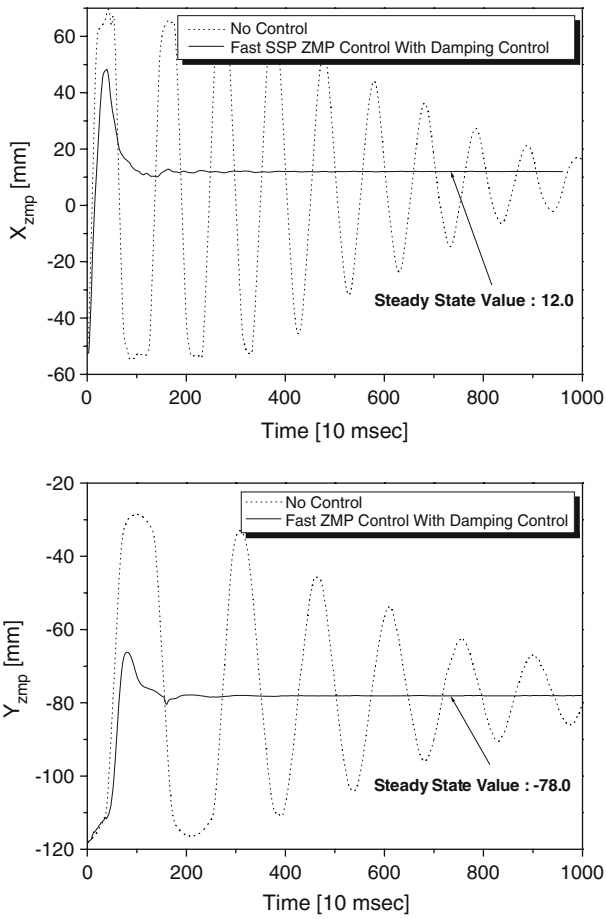

Fig. 27 A ZMP regulation comparison between the case of no control and the case of fast SSP ZMP compensation with the damping control

slow SSP ZMP compensator simultaneously. This strategy is not a general method. However, each compensator has a stable form without the poles in the RHP, hence it is possible to use both compensators simultaneously without the divergence. In this case, it can be seen that the ripples, overshoots and steady state errors are reduced suitably as shown in Fig. 29. Accordingly, the simultaneous use of the two different compensators was able to enhance the balance performance. In an actual case, during the single support phase, we divided the stability region into three parts according to the ZMP error, so in each part we applied one or both of the fast and slow SSP ZMP compensators. Figure 30 shows the control block diagram of SSP ZMP compensation. If the ZMP error is small, the fast SSP ZMP compensator alone is applied in order to follow the reference ZMP value rapidly. If ZMP error is large, only the fast SSP ZMP compensator also used because the slow SSP ZMP compensator might cause a large overshoot and falling down. If the ZMP error is moderate, both the fast and slow SSP ZMP compensators are used to stabilize the robot in the single support phase. Finally, these compensatory inputs are superimposed with the prescribed absolute pelvis trajectory.

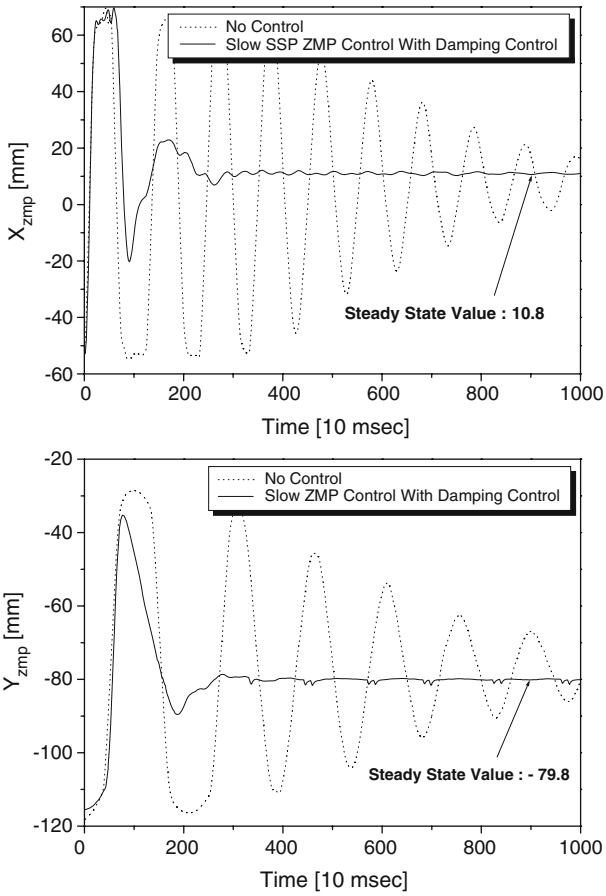

Fig. 28 A ZMP regulation comparison between the case of no control and the case of slow SSP ZMP compensation with the damping control

4.5 Landing Controller

In this part, we explain about the stable landing control strategy for dynamic stair climbing. The landing controller is composed of a landing altitude controller and a landing orientation controller. The landing altitude controller is described first.

4.5.1 Landing Altitude Controller

The landing altitude should be determined by considering the height of each stair. However, generally, the height of the stair is unknown and the attitude of the robot affects the landing altitude though we know the height of the stair; therefore, it is not desirable to define the constant landing altitude. If we know the height of the stair, this information is just used to determine at least how high the robot must lift its foot. Therefore, we developed the landing altitude controller for the suitable landing altitude of the swing foot. The principle is written as follows:

1. During lowering of the lifted swing foot, if the vertical floor reaction force more than 10 Kg is measured on the lowering foot before complete landing, robot

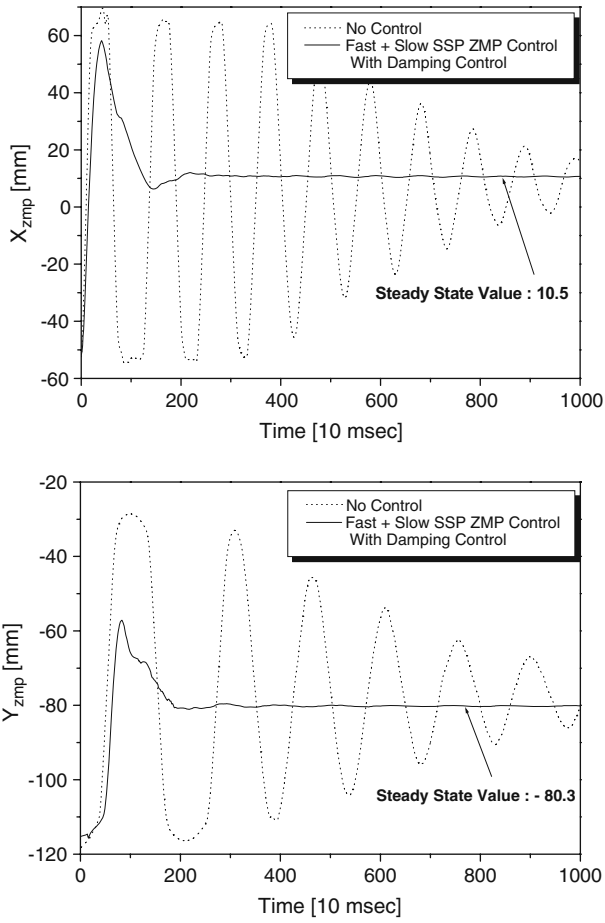

Fig. 29 A ZMP regulation comparison of the case of no control and the case of fast and slow SSP ZMP compensations with the damping control

stops and holds lowering of the swing foot. Then the swing foot becomes the supporting foot.

2. During lifting of the opposite foot (swing foot), robot lowers the supporting foot to the prescribed vertical position with respect to the body fixed coordinate frame through smooth cosine function.

In other words, the landing altitude controller switches the foot altitude pattern flow on or off according to the vertical reaction force during the second or fourth stage and pushes the landed foot down against the floor of the stair during the third or first stage (Fig. 31). Figure 32 shows relative vertical foot trajectories with respect to the body fixed coordinate. Since the origin of this coordinate is the pelvis center, the initial positions in z-direction of the two feet are -530 mm as shown in Fig. 5. In the first stage, the robot lifts the left foot, and then lowers the left foot in the second stage. During the second stage, the robot stops and holds lowering of the left foot when a vertical reaction force of 10 kg is detected at the force/torque sensor. After that, the robot is in the double support phase, so the DSP ZMP compensator stabilizes the robot during the rest of the second stage. From the start of the third

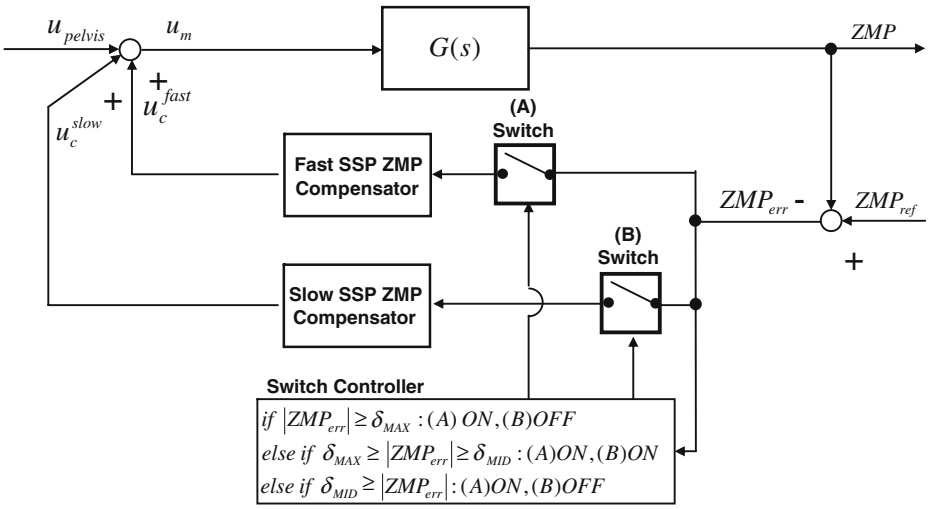

Fig. 30 A control block diagram of the SSP ZMP compensation

stage, the robot continues to lower the left foot to the prescribed foot height and lifts the right foot simultaneously. In this manner, KHR-2 can land its foot on suitable height each time despite of the change of the stair height or the variable attitude of the robot.

4.5.2 Landing Orientation Controller

This controller helps stabilize the landing by adjusting the angles of the ankle joints to the slope of the stair surface during the double support phase of the second or fourth stage. Generally, when the foot is landing, the slope of the sole is not same as that of the stair surface in the ground fixed coordinate frame. In this case, if we leave as it is, sudden instability will occur at the moment of contact, so, in the worst

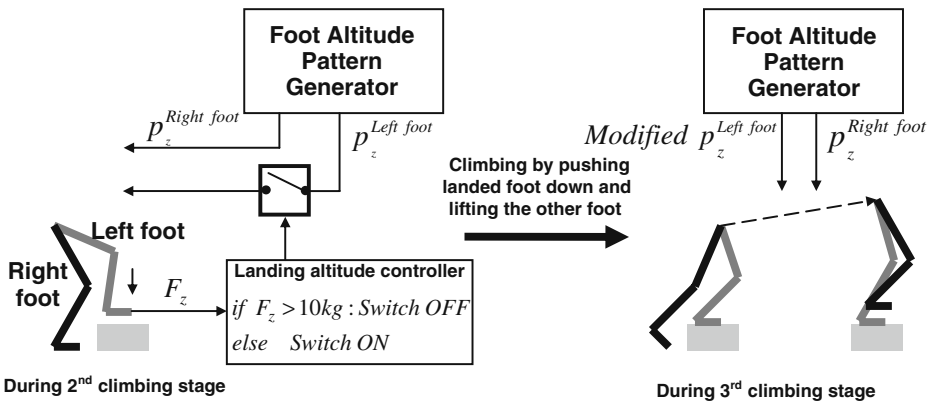

Fig. 31 Schematic of landing altitude controller

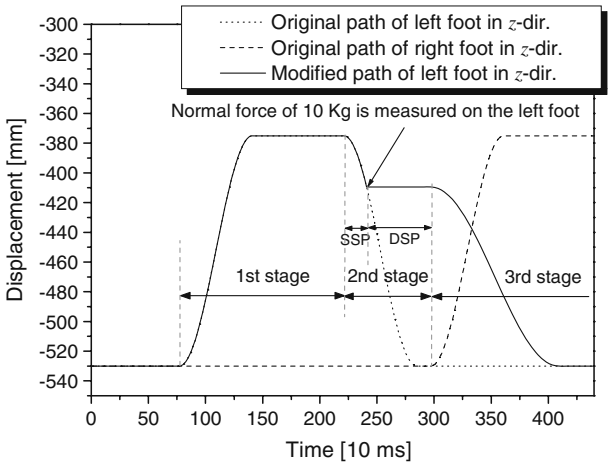

Fig. 32 Relative paths of two feet in vertical direction

case, the robot may fall down before climbing. Therefore, we have to compensate the angles of ankle joint so that the foot can be suitably adapted to the stair surface (Fig. 33). The principle is written as follows:

> If 1 kg of a vertical reaction force is detected on the landing foot, then virtual spring & damper systems at ankle roll and pitch joints are activated until 30 kg of a vertical reaction force is detected on the landing foot.

The control law of the landing orientation controller is based on the impedance control and written as follows:

$$z_1(s) = \frac{1}{m_1 s^2 + c_1 s + k_1} T_{pitch}(s)$$

$$z_2(s) = \frac{1}{m_2 s^2 + c_2 s + k_2} T_{roll}(s) \tag{21}$$

where, T_{pitch} *and* T_{roll} are the measured pitch and roll torques from the force/torque sensor, C_1 and C_2 are the damping coefficients, K_1 and K_2 are the stiffness. In Fig. 33, θ_{pitch} and θ_{roll} are the prescribed ankle pitch and roll joint trajectories. Finally, compensatory angles are superimposed to the prescribed ankle trajectories, so the ankle acts like a compliant joint which has torsional spring and damper systems. This

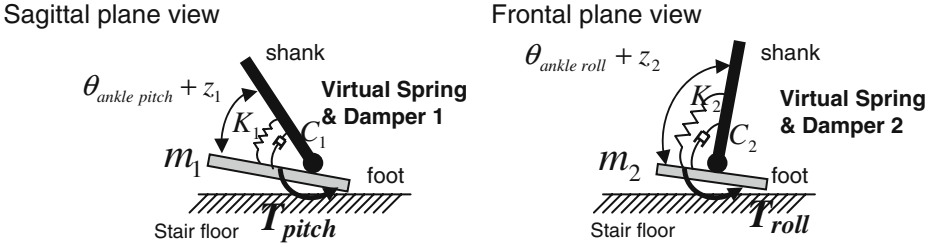

Fig. 33 Schematic of landing orientation control

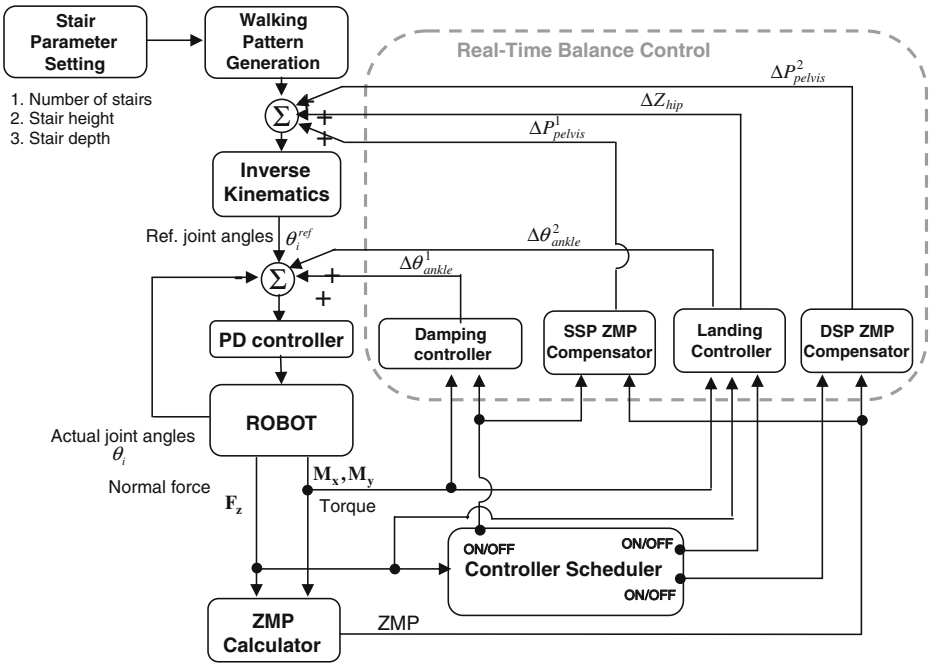

Fig. 34 The overall control flow diagram of stair climbing algorithm

controller is applied to the rolling and pitching joints of the ankles during the double support phase of the second or fourth stage.

4.6 Overall Control Strategy

The overall control flow diagram of the algorithm is represented in Fig. 34. Basically, after the stair parameter setting, the walking pattern is generated in real time. The

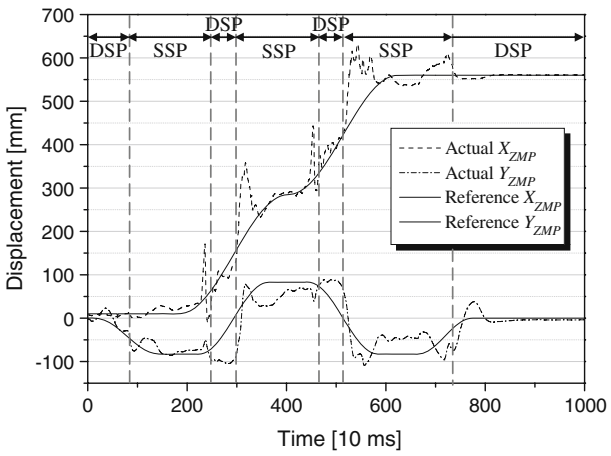

Fig. 35 Measurement of ZMP during dynamic stair climbing

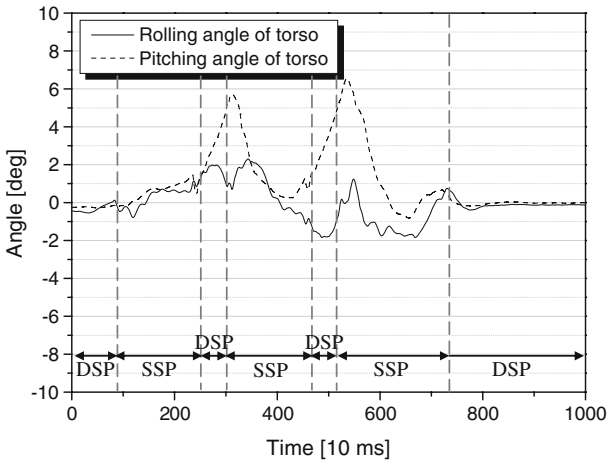

Fig. 36 Measurement of the inclination of the torso

walking pattern is modified by the ZMP compensators and the landing controller. The modified walking pattern is converted into the reference joint angles from the inverse kinematics. Also, the reference joint angles are modified again by the damping and the landing controllers. Finally, the PD controller controls each joint by the encoder feedback. All controllers use the force/torque sensor feedback. The damping controller and the landing orientation controller use the only torque data in order to modify the reference joint angle in the joint angle space, The ZMP compensators use the ZMP from the ZMP calculator in order to modify the pelvis displacement, and the landing altitude controller use the vertical ground reaction force in order to modify the landing height in the Cartesian space. All controllers are activated by the controller scheduler that uses the Table 4 and switches in Fig. 30.

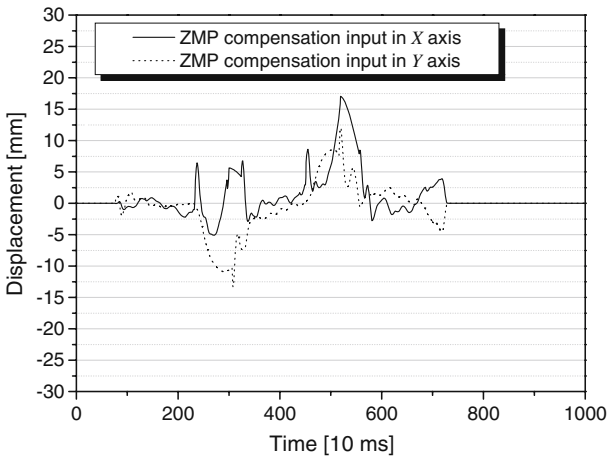

Fig. 37 Compensation inputs of ZMP compensators for pelvis horizontal motion

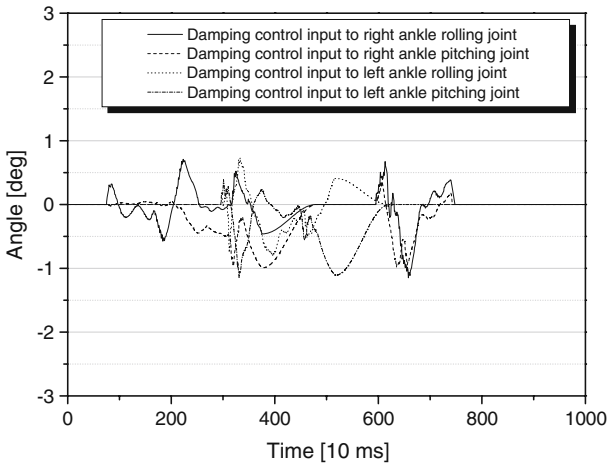

Fig. 38 Control inputs of damping controllers

5 Stair Climbing Experiments

We experimented with dynamic stair climbing by using KHR-2 in order to prove the effectiveness and the performance of the real-time balance control algorithm including online controllers. The height of each stair was 120 mm and the depth was 275 mm. In this experiment, we conducted a stair climbing with one walking cycle to verify the proposed algorithm. Figures 35 and 36 represent the ZMP and inclination of the torso during dynamic stair climbing. The torso inclination was measured through the use of the inertial sensor at the torso. In a lateral direction, the actual Y_{ZMP} followed reference Y_{ZMP} properly and the rolling angle of the torso was measured within just ± 2 degrees. The orientation of the torso was represented in Fig. 1. In a forward direction, the actual X_{ZMP} also followed reference X_{ZMP} well except ranges of 3.0–3.5 and 5.0–5.5 s. In these ranges, X_{ZMP} has a positive larger value than the reference X_{ZMP}, and this means that the robot was tilted forward for

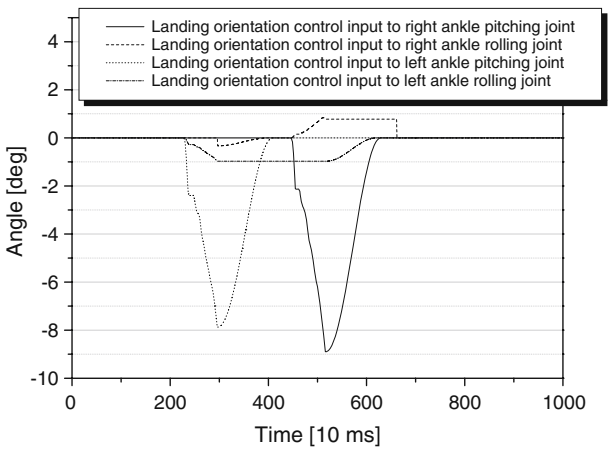

Fig. 39 Control inputs of landing orientation controllers

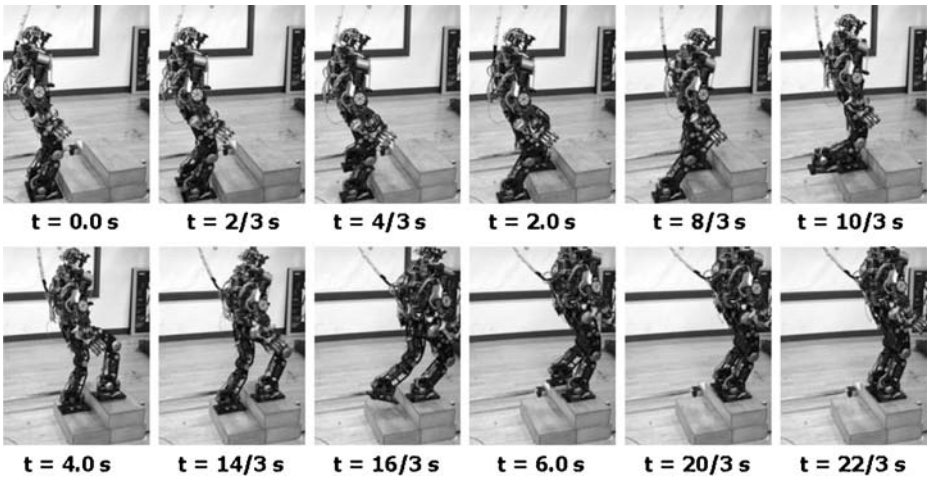

Fig. 40 Snapshot of the dynamic stair climbing of KHR-2

a short time of 0.5 s. We can easily verify the inclination by observing Fig. 36. In Fig. 36, there were two peaks with about 6° at those ranges too. Moreover, when we take a close look at Fig. 39, compensatory pitching angles of ankles have peaks at the same ranges. Therefore it can be known that these two peaks in X_{ZMP} and the pitching angle of the torso were cause by the landing orientation controller which causes robot to be tilted forward during the double support phases of the second or fourth stage. If the robot is not tilted forward at the moment of floor contact, it will definitely fall down backward. This is the way human do. After the complete landing, X_{ZMP} followed its reference and the pitching inclination of the torso went to zero quickly. The control inputs of ZMP compensators, damping controllers, and landing orientation controllers are plotted in Figs. 37, 38, and 39. In Fig. 37, the displacement for ZMP compensation was applied as pelvis horizontal motion on the transverse plane. In Figs. 38 and 39, control input angles were superimposed and applied to the rolling and pitching joints of the ankles. At present, we have succeeded in the dynamic stair climbing of KHR-2 with good stability. A snapshot of the experiment is shown in Fig. 40.

6 Conclusion

We proposed the control algorithm using force/torque sensors for the dynamic stair climbing of a biped humanoid robot.

1. For this research, we developed our biped humanoid robot, KHR-2 as a test platform and briefly introduced its overall specification.
2. We designed standard stair climbing pattern according to the three essential factors which we defined and the stair configuration.
3. We defined the five stair climbing stages by dividing the standard stair climbing pattern into five parts by considering the dynamic states of the robot.

4. We proposed a real-time balance control strategy, designed three kinds of online controllers and proved their effectiveness experimentally.
5. The performance of the real-time control algorithm for dynamic stair climbing was successfully verified by experimentation.

In this research, we have researched the experimental realization of dynamic stair climbing using only force/torque sensors, but we will use other sensors such as an inertial sensor that is composed of rate gyros and accelerometers in order to prepare for a bad landing of the foot and to improve the stability of the attitude of the torso. A new problem in dynamic stair climbing is that the tiptoe of the swing foot may collide with the stair wall. If the collision occurs, the structural vibration of the torso is generated in a yawing direction and the direction of the stair climbing is changed a little. Therefore, it is important to eliminate the vibration quickly by a torso compliance control strategy. We will achieve torso compliance control by using the rate gyro of the torso. In addition, researches about the detection of stair dimensions, going downstairs, and advanced walking pattern generation that considers a complex dynamic model and a desired ZMP trajectory will be also performed as the future works.

For the generality, this dynamic stair climbing algorithm will be applied to our next version of biped robots such as HUBO, Albert HUBO and HUBO FX-1. A dynamic stair climbing movie of KHR-2 can be seen on the web site (http://www.hubolab.com).

References

1. Lim, H., Kaneshima, Y., Takanishi, A.: Online walking pattern generation for biped humanoid robot with trunk. In: Paper Presented at the IEEE International Conference on Robotics and Automation, Washington, DC, USA, 11–15 May 2002
2. Kim, J.Y., Park, I.W., Lee, J., Kim, M.S., Cho, B.K., Oh, J.H.: System design and dynamic walking of humanoid robot KHR-2. In: Paper Presented at the IEEE International Conference on Robotics and Automation, Barcelona, Spain, 18–22 April 2005
3. Hirai, K.: Current and future perspective of Honda humanoid robot. In: Paper Presented at IEEE/RSJ International Conference on Intelligent Robots and Systems, Grenoble, France, 7–11 September 1997
4. Nishiwaki, K., Kagami, S., Kuniyoshi, Y., Inaba, M., Inoue, H.: Online generation of humanoid walking motion based on fast generation method of motion pattern that follows desired ZMP. In: Paper Presented at IEEE/RSJ International Conference on Intelligent Robots and Systems, Lausanne, Switzerland, 30 September–5 October 2002
5. Kajita, S., Kanehiro, F., Kaneko, K., Hujiwara, K., Harada, K., Yokoi, K., Hirukawa, H.: Biped walking pattern generation by using preview control of zero-moment point. In: Paper Presented at the IEEE International Conference on Robotics and Automation, Taipei, Taiwan, 14–19 September 2003
6. Pfeiffer, F., Löffler, K., Gienger, M.: The concept of jogging johnnie. In: Proc. IEEE Int. Conf. Robot. Autom. **3**, 3129–3135 (2002)
7. Vukobratovic, M., Borovac, B., Surla, D., Stokic, D.: Biped Locomotion. Springer, Berlin (1990)
8. Kajita, S., Nagasaki, T., Kaneko, K., Yokoi, K., Tanie, K.: A running controller of humanoid biped HRP-2LR. In: Proc. IEEE Int. Conf. Robot. Autom. 616–622 (2005)
9. Hodgins, J.K., Raibert, M.N.: Adjusting step length for rough terrain locomotion. IEEE Trans. Robot. Autom. **7**(3), 289–298 (1991)
10. Shih, C.L.: Ascending and descending stairs for a biped robot. IEEE Trans. Syst. Man Cybern. **29**(3), 255–268 (1999)

11. Figliolini, G., Ceccarelli, M.: Climbing stairs with EP-WAR2 biped robot. In: Paper Presented at the IEEE International Conference on Robotics and Automation, Seoul, Korea, 21–26 May 2001
12. Nishiwaki., K., Kagami., S., Kuniyoshi., Y., Inaba., M., Inoue, H.: Toe joint that enhance bipedal and full body motion of humanoid robots. In: Paper Presented at the IEEE International Conference on Robotics and Automation, Washington, DC, USA, 11–15 May 2002
13. Jeon, K.S., Kwon, O., Park, J.H.: Optimal trajectory generation for a biped robot walking a staircase based on genetic algorithms. In: Paper Presented at IEEE/RSJ International Conference on Intelligent Robots and Systems, Sendai, Japan. 27 September–1 October (2004)
14. Kim, S.H., Sankai, Y.: Stair climbing task of humanoid robot by phase composition and phase sequence. In: Paper Presented at the IEEE International Workshop on Robotics and Human Interactive Communication, Nashville, TN, USA, 13–15 August 2005
15. Takahashi, Y., Nakayama, H., Nagasawa, T.: Biped robot to assist walking and moving up-and-down stairs. In: Paper Presented at IEEE 24th Annual Conf. of Industrial Electronics Society, Aachen, Germany, 31 August–4 September 1998
16. Sugahara, Y., Ohta, A., Hashimoto, K., Sunazuka, H., Kawase, M., Tanaka, C, Lim, H., Takanishi, A.: Walking up and down stairs carrying a human by a biped locomotor with parallel mechanism. In: Proc. IEEE/RSJ Int. Conf. Intell. Robot Syst. 1489–1494 (2005)
17. Figliolini, G., Ceccarelli, M.: EP-WAR3 biped robot for climbing and descending stairs. Robotica **22**(4), 405–417 (2004)
18. Nishiwaki, K., Kagami, S.: Sensor feedback modification methods that are suitable for the short cycle pattern generation of humanoid walking. In: Proc. IEEE/RSJ Int. Conf. Intell. Robot Syst. 4214–4220 (2007)
19. Kim, J.Y., Park, I.W., Oh, J.H.: Experimental realization of dynamic walking of biped humanoid robot KHR-2 using ZMP feedback and inertial measurement. Adv. Robotics **20**(6), 707–736 (2006)
20. Inman, V.T., Ralston, H.J., Todd, F.: Human Walking. Williams & Wilkins, London (1981)
21. Kim, J.H., Oh, J.H.: Walking Control of the Humanoid Platform KHR-1 based on Torque Feedback Control. In: Paper Presented at the IEEE International Conference on Robotics and Automation, New Orleans, LA, 26 April–1 May 2004
22. Chen, C.T.: Linear system theory and design 3rd edn. Oxford Press, New York (1999)